New insights in copper handling strategies in the green alga *Chlamydomonas reinhardtii* under low-iron condition

Emeric Kochoni,[1,2] Imad Aharchaou,[1,2] Leanne Ohlund,[3] Maikel Rosabal,[2,4] Lekha Sleno,[2,3] and Claude Fortin[1,2]

[1]Institut National de la Recherche Scientifique, Centre Eau Terre Environnement, 490, rue de la Couronne, Québec, QC, G1K 9A9, Canada. E-mail: claude.fortin@ete.inrs.ca
[2]EcotoQ, 490, rue de la Couronne, Québec, QC, G1K 9A9, Canada
[3]Département de Chimie, Université du Québec à Montréal (UQAM), 2101, rue Jeanne-Mance, Montréal, QC, H2X 2J6, Canada
[4]Département des Sciences biologiques, Université du Québec à Montréal (UQAM), 141 Avenue du Président-Kennedy, Montréal, QC, H2X 1Y4, Canada

Published in Metallomics (07 May 2022)

10.1093/mtomcs/mfac033

Key words: Detoxification mechanisms, phytochelatins, subcellular distribution, copper binding proteins, metallomics, proteomics.

Running head: Algal copper trafficking under low-Fe condition

Abstract

Copper (Cu) is a redox-active transition element critical to various metabolic processes. These functions are accomplished in tandem with Cu binding ligands, mainly proteins. The main goal of this work was to understand the mechanisms that govern the intracellular fate of Cu in the freshwater green alga, *Chlamydomonas reinhardtii,* and more specifically to understand the mechanisms underlying Cu detoxification by algal cells in low-Fe conditions. We show that Cu accumulation was up to 51-fold greater for algae exposed to Cu in low-Fe medium as compared to the replete-Fe growth medium. Using the stable isotope ^{65}Cu as a tracer, we studied the subcellular distribution of Cu within the various cell compartments of *C. reinhardtii*. These data were coupled with metallomic and proteomic approaches to identify potential Cu-binding ligands in the heat-stable proteins and peptides fraction of the cytosol. Cu was mostly found in the organelles (78%), and in the heat-stable proteins and peptides (21%) fractions. The organelle fraction appeared to also be the main target compartment of Cu accumulation in Fe-depleted cells. As Fe levels in the medium were shown to influence Cu homeostasis, we found that *C. reinhardtii* can cope with this additional stress by utilizing different Cu-binding ligands. Indeed, in addition to expected Cu-binding ligands such as glutathione and phytochelatins, 25 proteins were detected that may also play a role in the Cu detoxification processes in *C. reinhardtii*. Our results shed new light on the coping mechanisms of *C. reinhardtii* when exposed to environmental conditions that induce high rates of Cu accumulation.

Significance to metallomics

This work analyzes not only the intracellular distribution of Cu in the green alga *Chlamydomonas reinhardtii*, but also the mechanisms that govern its detoxification. These mechanisms involve the activity of biomolecules, often proteins, which interact with Cu (or other metals) through functional groups (-SH, -NH, -OH or COOH). The analysis of these Cu-ligand complexes using metallomics and proteomics approaches makes it possible to identify or infer their cellular functions.

Graphical abstract

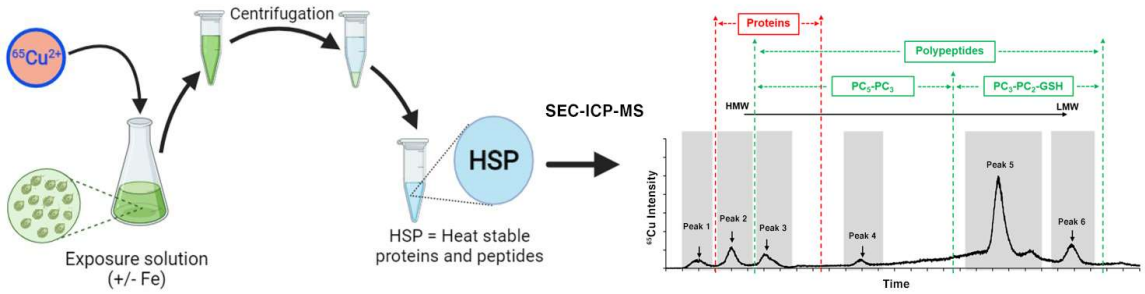

Cells were exposed to copper, harvested, lysed and the heat-stable proteins and peptides were isolated. Copper was then determined by inductively coupled plasma mass spectrometry after separation by size exclusion chromatography.

1 Introduction

Modeling of a system requires an understanding of the phenomena that take place and an ability to quantify them in order to subsequently predict (anticipate) them. Modeling can be used to overcome certain technological constraints and reduce delays, and above all, limit project costs and fill gaps between scientific progress and regulation applicability. In ecotoxicology, the emergence and development of predictive models, such as the Biotic Ligand Model (BLM), improved not only our comprehension of aqueous metal bioavailability, but also the potential interactions between chemicals (metals and ligands) and the effects upon aquatic organisms [1]. Taking into account the effects of aquatic physicochemical parameters (ionic composition, pH, dissolved organic carbon) on metal bioavailability is increasingly considered in environmental regulation [2, 3]. Despite these advances in our capacity to predict metal bioavailability, several aspects of physiologic mechanisms governing trace metal interactions with aquatic organisms remain unclear, such as metal interference with cell metabolism and metal homeostasis [3].

It was shown that in freshwater algae, trace essential elements can also play a role in metal bioavailability and homeostasis [4-6]. Recently, we showed that the concentration of iron (Fe^{3+}) in water has an effect on copper (Cu^{2+}) accumulation and toxicity in the freshwater green alga, *C. reinhardtii* [7]. We showed that a typical culture medium concentration of Fe^{3+} ($[Fe^{3+}]_{free} \approx 10^{-18}$ M) had a protective effect against Cu toxicity, while a lower concentration ($[Fe^{3+}]_{free} \approx 10^{-19}$ M) resulted in hypersensitivity to Cu. These observations, also reported in marine diatoms [8, 9], raised several questions: How can Fe deficiency induce Cu hypertoxicity in algae? What are the fundamental mechanisms underlying this Cu toxicity at low ambient Fe? And what detoxifying mechanisms are triggered in algal cells to cope with this situation? The objective of the present study was to understand how the concentration of Fe affects Cu intracellular fate and homeostasis in *C. reinhardtii*. More specifically, the aim was to study the subcellular distribution of Cu at low and replete Fe^{3+} levels in the growth medium and to characterize the Cu binding ligands involved with its detoxification in *C. reinhardtii*. Cu and Fe homeostasis is a well-studied process in *C. reinhardtii*. It involves various families of transporters and metallochaperones. For example, several members of the FTR (Fe transporters) and CTR (Cu transporters) family

have been identified and transport Fe and Cu, respectively (for reviews see Blaby-Hass and Merchant, Glaesener *et al.*, Hanikenne *et al.*, Kropat *et al.* and Merchant *et al.* [10-15]). Metal detoxification mechanisms in algae are well documented and involve biomolecules rich in thiol groups such as cysteine (Cys), glutathione (GSH) and phytochelatins (PCs) [16, 17]. According to [18] and [19], these biomolecules are expected to be found in the HSP (heat stable proteins and peptides) fraction following a subcellular fractionation scheme. We therefore hypothesized that Cu is mainly complexed by organic ligands rich in –SH, and thus is predominantly contained in the HSP fraction. Our methodological approach consisted of several investigation techniques and biomolecular analyses using *C. reinhardtii* as a model. First, Cu subcellular fractionation was carried out on the algal cells. Second, using only the HSP fraction, metallomics and proteomics analyses were conducted [20-22] for molecular characterization of the Cu-binding ligands present in this cell compartment.

2 Materials and methods

2.1 Test organism and growth conditions

The freshwater unicellular green alga *Chlamydomonas reinhardtii* (CPCC11 strain, wild type) was obtained from the Canadian Phycological Culture Centre (University of Waterloo, ON, Canada). Axenic cultures were maintained in a good physiological state in modified high salt medium (MHSM1, Table S1; Supplementary Material) at pH 7 in 250-mL Erlenmeyer flasks as described in [18] and [19]. In the present work, we used ^{63}Cu as a Cu source to prepare the MHSM1 medium to obtain algae cells with a Cu signature dominated by ^{63}Cu. The cells were cultured in an environmental growth chamber (Conviron, CMP4030) under constant conditions (continuous illumination of 100 $mol \cdot m^2 \cdot s^{-1}$, temperature maintained at 20.0 ± 0.2 °C, and rotary agitation of 100 rpm; see [7] for more details). The culture was refreshed once a week under the same conditions presented above. Two batches of algal cells were compared in this work depending on their growth conditions, i.e. if they were acclimated to a low-Fe or replete-Fe condition. The non-acclimated cells to replete Fe conditions (M-algae) were grown in replete-Fe medium (MHSM1 medium, $[Fe^{3+}]_{free} = 10^{-18}$ M, Table S1; Supplementary Material). The low-Fe acclimated algae (L-algae) were grown prior to the exposure experiments in a low-Fe

condition (LM1 medium, $[Fe^{3+}]_{free} = 10^{-19}$ M, Table S1; Supplementary Material). The use of the term "low" refers to the lowest Fe concentration we could use while maintaining normal algal growth and the term "replete" was used for cells grown at Fe levels found in the routine growth medium. Additionally, the culture was kept in the exponential phase for about 8 days by refreshing it twice a week under the low-Fe condition. For the last transfer, which took place 48 to 72 h before exposure to Cu, 10 to 20 mL of culture was transferred into 500 mL of MHSM1 or LM1 medium for M-algae and L-algae, respectively. This step was done in a 1-L Erlenmeyer flask in order to have a sufficient number of cells for the exposure experiments (see below). All culture glassware and media were autoclaved at 121 °C for 15 min before use.

2.2 Exposure conditions of algae cells to Cu

Unless otherwise mentioned, cells were exposed to ^{65}Cu ($[^{65}Cu^{2+}]_{free} = 3.55$ nM). Exposure media were specifically designed for each exposure condition. Two exposure times (2 and 72 h) were performed and two treatments (low-Fe and replete-Fe exposure medium) were compared (Figure S1; Supplementary Material). Tables S2 and S3 (Supplementary Material) show the detailed ionic composition of the exposure media, both for total and calculated free ion concentrations. A total of four samples were processed per exposure experiment: one control and three replicate treatments.

Before the initiation of the exposure experiments, algal cells that were grown in 500 mL of culture medium (MHSM1 or LM1) were collected by filtration on a 2-µm polycarbonate filter (Isopore TM, Merck Millipore), rinsed three times with 10 mL of the rinse solution (see LM-R in Table S2; Supplementary Material) and suspended in a new 50 mL tube containing 20 mL of the rinse solution. Then, the exact volume needed of the re-suspended algae were determined and added to 400 mL of the exposure medium to achieve *in fine* a cell density of approximately 150 000 cell·mL^{-1}. The cell density was then determined using a particle counter (Multisizer TM 3 Coulter Counter®; Beckman) and noted. The exposures were carried out in 500 mL tubes previously washed with acid (10% HNO_3, v/v) for 24 h, rinsed three times first with deionized water then with milli-Q water (resistivity > 18.2 MΩ·cm; total organic carbon < 2 µg·L^{-1}), and autoclaved (15 min, 121 °C) before use. A Teflon-coated magnetic bar was placed in each tube, which was then placed on a stirrer

for the entire duration of the exposure, which took place at room temperature (20-22 °C) and under constant brightness (lab light i.e. 15.3 ± 3.4 µE or $\mu mol \cdot m^{-2} \cdot s^{-1}$). At the end of each exposure, 4 mL of ethylenediaminetetraacetic acid (EDTA; 0.1 M) was added to each tube to bind virtually all the trace metals (including $^{65}Cu^{2+}$) still present in the exposure media and thus stop their transfer in the cells [23].

2.3 Subcellular fractionation procedure

In order to determine the distribution of Cu inside algal cells, subcellular fractionation was performed according to the procedure elaborated specifically for *C. reinhardtii* by [24] which was elaborated to minimize metal migration and cross-contamination of fractions. At the termination of the exposures, 400 mL of the exposed algae suspension was centrifuged (Sorwall® RC 5C Plus, Du Pont) for 10 min at 9 000 rpm and 20-22 °C. The supernatant was then removed from each container and a volume of approximately 30 mL was left in the bottles. Pellets were then re-suspended and transferred to 30 mL centrifuge tubes. These tubes were centrifuged for 4 min at 9 000 rpm and 20-22 °C. When the centrifugation was completed, the supernatant was removed, leaving only the pellet at the bottom of the tube. Cells were then re-suspended in 10 mL of the rinse solution (LM-R, Table S2; Supplementary Material), centrifuged four times (9 000 rpm, 4 min, 20-22 °C) and re-suspended each time in 10 mL of rinse solution. At each step of this process, 4 mL aliquots of the exposure solution and of the supernatant were filtered (using 25 mm sterile syringe filters (Polyethersulfone Membrane); 0.45 µm porosity (VWR International)) and collected for ^{65}Cu analyses. After the last centrifugation, algal cells were collected and re-suspended in 2 mL of rinse solution in 7 mL polypropylene tubes. Aliquots of 0.5 mL of the re-suspended cells were set aside, from which 20 µL were used to determine the exact cell density of the final suspension. The rest of the cells were harvested and mineralized in order to determine the total intracellular metal concentration and perform a mass balance calculation. The remaining ~1.5 mL of the final algal suspension was homogenized at low temperature (4 °C, or under ice) by using an ultra-sonicator (Branson SFX150, Danbury, CT, U.S.A.) for 4 min (power = 22 W; pulse = 0.2 s/s) in order to lyse the cells. To make sure that cells were broken efficiently, cell size was determined (using a particle counter) before and after sonication. The homogenates were then put in 3 mL ultracentrifugation

Eppendorf tubes and weighed to obtain the exact volume of cell homogenate suspension. A differential centrifugation process designed to separate different subcellular fractions (Figure S2; Supplementary Material) was then conducted to separate the following five subcellular fractions: (*i*) debris (DB: nuclei, cell membranes, cell walls), (*ii*) granules-like (GR: NaOH-resistant materials), (*iii*) organelles (ORG: mitochondria, Chloroplast/Pyrenoid, Golgi apparatus, endoplasmic reticulum), (*iv*) heat-stable proteins and peptides (HSP: GSH, PCs and other unidentified thermostable peptides) and (*v*) heat-denatured proteins (HDP: enzymes) (see Figure S2; Supplementary Material). Note that, metal accumulation in the DB fraction was not included in our discussion as the current state of knowledge of its toxicological significance is not well defined [25, 26].

As illustrated in Figure S2 (Supplementary Material), once broken, homogenized samples were centrifuged at 1500 g at 4 °C for 15 min. The supernatant (S1), comprising a mixture of organelles and cytosolic solution, was transferred to another Eppendorf tube and again centrifuged at 100 000 g at 4 °C for 60 min. The pellet (P1) was re-suspended in 0.5 mL of Milli-Q water and heated in the oil bath at 100 °C for 2 min and then transferred to another oil bath at 70 °C for 10 min. After that, 0.5 mL of KOH (1 M) was added and further heated in the oil bath at 70 °C for 60 min, followed by centrifugation at 10 000 g and 4°C for 15 min. The resultant supernatant (S2), which constitutes the DB fraction, was transferred to a 13-mL tube while the pellet (P2) provided the GR fraction. The original S1 supernatant was then ultracentrifuged for 60-min to provide supernatant (S3), which is the cytosolic fraction, and pellet (P3), which constitutes the ORG fraction. The supernatant S3 was then transferred to an Eppendorf tube, placed in an oil bath at 80 °C for 10 min and transferred to an ice bath for 60 min, which easily allows the HDP fraction to be separated from the HSP fraction. As for the pellet (P3), it was set aside for mineralization. After 60 min on ice, supernatant S3 was centrifuged at 50 000 g (4°C, 15 min), and the supernatant (S4) was transferred to a 13-mL tube and the pellet (P4), which is the HDP fraction, was kept in the tube and put aside until the mineralization step. All centrifugation steps were performed using a WX ultra series centrifugation (Thermo Scientific).

2.4 SEC-ICP MS analyses and Cu speciation

Coupling of size exclusion chromatography with inductively coupled plasma mass spectrometry (SEC-ICP-MS) was used to separate the biomolecules present in the HSP fraction [27]. The aim of this experiment was to determine the Cu distribution among different molecular weight pools inside the HSP fraction of the cells to get insight into the biomolecules involved in Cu detoxification mechanisms in *C. reinhardtii*. These HSP fractions were obtained by applying a subcellular fractionation protocol as described in the earlier section (Subcellular fractionation procedure) with some modifications. Briefly, algae were exposed to 39.3 nM of free $^{65}Cu^{2+}$ (in order to obtain and distinguish ^{65}Cu signal from background noise) and, at the end of the rinse steps (see section 2.3), algal cells were homogenized in a fresh ammonium acetate buffer (100 mM, pH 7.4). Then, 1.5 mL of each homogenate sample was subjected to ultracentrifugation (100 000 g, 60 min, 4 °C) to isolate the cytosol (supernatant) from the rest of the cell contents (pellet). The supernatant (cytosol) was then transferred to a new Eppendorf tube, and was heated (80 °C, 10 min), cooled (4 °C, 60 min) and re-subjected to a final ultracentrifugation step (50 000 g, 15 min, 4 °C) to collect heat-stable proteins and peptides present in the final supernatant (HSP fraction).

Size-exclusion chromatographic (SEC) separation of the HSP fractions (n = 3 per treatment) was performed on a Thermo Spectra HPLC system (Thermo Fisher Scientific, Winsford, England, UK) equipped as described previously in [27]. The SEC column, Superdex^{TM} 30 Increase 10/300 GL (GE Healthcare Bio-Sciences AB, Uppsala, Sweden), with a size separation range of 0.1 to 7 kDa, was used to elute samples with 100 mM ammonium acetate buffer (pH 7.4) at a flow rate of 0.7 mL·min^{-1}. Before each analysis and between each run, the column was washed for 45 min with 150 µL of 10 mM EDTA-Cys buffer (pH 7.4) to remove any metal ions adsorbed on the stationary phase and avoid potential cross contamination of samples. For each injection, 200-250 µL of sample was run through the column, and absorbance at 280 and 254 nm was measured (as an indication of the presence of proteins and peptides respectively). Then, the ^{65}Cu signal was monitored in real time by coupling an ICP-MS (XSERIES 2, Thermo Fisher Scientific, Winsford, England, UK) to the SEC system. The ^{65}Cu intensity (number of counts) was recorded and plotted as a function of the retention time (RT) in order to reveal Cu-ligand peaks in each

HSP aliquot injected. In addition to the ^{65}Cu signal, the signals of ten other masses (corresponding to ^{60}Ni, ^{63}Cu, ^{64}Zn, ^{65}Cu, ^{75}As, ^{77}ArCl, ^{82}Se, ^{83}Kr, ^{111}Cd, ^{208}Pb) were also monitored simultaneously as quality control. The Superdex column was calibrated with several molecular weight standards and the molecular masses of Cu-biomolecule complexes contained in the HSP fractions were then estimated by using the molecular weight calibration graph. SEC-ICP-MS analyzes in HSP fractions were conducted in triplicate for each treatment tested.

To collect the samples destined for proteomic and peptidomic analyses, 200 µL of the HSP fraction were first injected in duplicate into the SEC-ICP-MS system to locate the RT of the ^{65}Cu-protein/peptide complexes (from Cu1 to Cu6). Then, the ICP-MS was disconnected from the HPLC, and for the eight subsequent injections, all localized peaks were separately collected based on their RT in 50 mL tubes (Falcon Conical Centrifuge Tubes), frozen and lyophilized. At the end of the lyophilization process, the content of each tube was re-suspended in 1 mL of milli-Q water and stored at -20 °C until the proteomic and peptidomic analyses.

2.5 LC-MS/MS analyses of SEC fractions

2.5.1 Targeted phytochelatin and glutathione (peptide) analyses

2.5.1.1 Sample preparation

Sample fractions (190 µL) were mixed with 10 µL of 100 mM dithiothreitol (DTT Sigma-Aldrich, Oakville, ON, CA). Standard solutions (10 µM) of GSH, PC2 and PC6 (PCs with two and six thiol groups) with 5 mM final DTT concentration were also prepared (Table 1). Samples (20-30 µL) and standards (10 µL) were analyzed by high performance liquid chromatography-quadrupole time of flight mass spectrometry (HPLC-QqTOF-MS), on a Shimadzu Nexera UHPLC coupled to a Sciex TripleTOF 5600 system equipped with a DuoSpray ion source in negative ion mode with 4.5 kV source voltage, 500 °C source temperature, 35 psi curtain gas and 50 psi GS1/GS2 gas flows, and a declustering potential of 80 V. Separation of components was performed using two different columns and methods. The first column used was an Agilent (Santa Clara, CA, U.S.A.) Eclipse C18 (2.1 x 50 mm, 1.8 µm) with mobile phases of water (A) and acetonitrile (B), both containing

0.1% formic acid, at 40 °C and a flow rate of 0.5 $mL \cdot min^{-1}$. The elution gradient employed was as follows: 5% B held for 0.5 min, then increased linearly to 30% B at 8 min, up to 80% B at 10 min and held for 1 min before re-equilibrating at 5% B for 5 min before the next injection (Table 1). The second chromatographic column employed was an Imtakt (Portland, OR, U.S.A.) Scherzo SM-C18 (150 x 3 mm, 1.8 µm) with mobile phases of water (A) and acetonitrile (B), both containing 0.1% formic acid, at 40 °C and a flow rate of 0.25 $mL \cdot min^{-1}$. The elution gradient employed was as follows: 3% B held for 3 min, then increased linearly to 95% B at 15 min and held for 1 min before re-equilibrating at 3% B for 8 min before the next injection (Table 1).

2.5.1.2 Sample analyses

Both TOF-MS and MS/MS analyses were performed using electrospray ionization (ESI) in negative mode with the mass range of *m/z* 100-1200 and *m/z* 40-800, respectively. To ensure accurate mass measurements, the instrument was calibrated every four injections with a mix of standard compounds covering a range of *m/z* from 100 to 1000. Manual data verification and visualization were done with PeakView 2.2 and MasterView 1.1 (Sciex).

2.5.2 Proteomic analyses

2.5.2.1 Sample preparation

Molecular weight cut-off (MWCO) filtration was used to concentrate SEC fractions 1 to 3 (SEC fractions correspond to Cu peaks obtained after the HSP fraction was subjected to SEC-ICP-MS analyses and collected in separate tubes). Aliquots of 500 µL of each fraction containing approximately 10-15 µg of proteins were concentrated to 25 µL with 10 kDa Amicon MWCO filters (Millipore-Sigma, Burlington, MA, U.S.A.).

2.5.2.2 Trypsin digestion

Concentrated samples were diluted with 250 µL of 100 mM ammonium bicarbonate buffer (ABC) at pH 8.5 and 10 µL of 100 mM dithiothreitol, incubated at 37 °C for 20 min, followed by alkylation with 15 µL of 100 mM iodoacetamide (Sigma-Aldrich, Oakville, ON, Canada) in the dark at 37 °C for 30 min. Trypsin (10 µL of 0.1 $mg \cdot mL^{-1}$ solution) (Sigma-Aldrich) was added to each sample and incubated overnight at 37 °C. Digested samples were cleaned up by solid phase extraction using Oasis HLB cartridges (1 cc, 30

mg, Waters, Milford, MA) with methanol elution. Dried extracts were reconstituted in 100 µL 10% acetonitrile prior to LC-MS/MS analyses.

2.5.2.3 LC-MS/MS analyses and data processing

Samples were injected (30 µL) onto an Aeris PEPTIDE XB-C18 100 × 2.1 mm, 1.7 µm column, with a SecurityGuard ULTRA C18-peptide guard column (Phenomenex, Torrance, CA) using a Nexera UHPLC system (Shimadzu, Columbia, MD) with water (A) and acetonitrile (B), both containing 0.1% formic acid, as a mobile phase at the flow rate of 0.3 $mL \cdot min^{-1}$ (40 °C). The gradient started at 5% B, was held for 2.5 min, and was linearly increased to 30% B at 24 min, to 50% B at 26 min, to 85% B at 26.55 min, then to 95% B at 26.6 min and held there for 1.5 min, and re-equilibrated for 8.5 min between injections.

High-resolution TOF-MS and MS/MS analyses were performed on a hybrid QqTOF-MS, TripleTOF 5600 (Sciex, Concord, ON, Canada), equipped with a DuoSpray ion source in positive mode with 5 kV source voltage, 500 °C source temperature, 35 psi curtain gas and 50 psi GS1/GS2 gas flows, and declustering potential of 80 V. TOF-MS acquisition was from *m/z* 120-1250 followed by data-dependant MS/MS acquisition on the 15 most intense ions from *m/z* 80-1500 with dynamic background subtraction and a collision energy of 30 ± 10 V. Protein Pilot 5.0.2 (Sciex) was used to search LC-MS/MS data against a *C. reinhardtii* protein database downloaded from Uniprot.org (September, 2020) with a set of common contaminant proteins added. Proteins and peptides were identified with a local 1% false discovery rate (FDR) using a target-decoy database search algorithm. ProteinPilot search results were loaded into Scaffold v4 (Proteome Software) to compare protein and peptide IDs across the samples.

2.6 Element determinations and controls

Concentrations of ^{65}Cu and Fe in the media, the subcellular fractions and the cells were determined following the mineralization step (HNO_3 10%, Trace Metal Grade and H_2O_2, Optima Grade) by using ICP-MS and inductively coupled plasma atomic emission spectrometry (ICP-AES, Varian Vista AX), respectively. Cu content in algae was corrected using the signal from control algae (not exposed to ^{65}Cu), which was always less than 2%.

Unless otherwise indicated, all experiments were performed in triplicate and the quality assurance and control were done as described in previous work (see [7]). The Cu stable isotopes (^{63}Cu and ^{65}Cu) used to design the culture and exposure media were 99% pure (Trace Sciences International, Canada). For ICP analyses, Fisher certified reference standards were used, and the repeatability of values obtained by ICP were ≥ 97%. In addition, the calibration curves, used to quantify metals by the both ICP instruments, were prepared with single standard elements (SCP Science). For the quality control, multi-elemental certified standards (900-Q30-100, SCP Science) and a proficiency testing study for trace elements in water (#TE105-05, Environment and Climate Change Canada) were used and the recovery levels of each control material were 99.6 ± 4.6% (n = 22) and 110.5 ± 5.1% (n = 22), respectively. The mass balances of Cu were performed after the subcellular experiment by comparing the sum of ^{65}Cu contained in the various subcellular fractions with the total of ^{65}Cu inside algal cells. The average recovery for Cu mass balances obtained after subcellular fractionation was 90 ± 17% (n = 12). Cell densities, sizes, and surface distributions were determined using a particle counter (Multisizer TM 3 Coulter Counter®; Beckman). The chromatographic recovery of SEC system used was performed by comparing Cu amount injected versus collected in the presence and absence of the column and this recovery reached 96.8 %.

2.7 Statistics and data treatment

All numerical data are shown as means ± 1 standard deviation (SD); n = 3, unless otherwise mentioned. Statistically significant differences among treatments were determined by using a nonparametric test (Kruskal-Wallis) and a Tukey honestly significant difference (HSD) test was performed on ranks to discriminate among treatments. All conclusions are based on at least a 5% level of significance ($p > 0.05$). Unless specified, all statistical tests were performed using JMP Pro 13.0.0 software (SAS Institute, Riverside, CA, U.S.A.) and graphs were produced by using the MS Excel 2016 and Sigma Plot 12.5 (Systat Software, Inc., U.S.A.). Error propagation was calculated each time measured values were pooled.

3. Results and discussion

3.1 Cu accumulation in *C. reinhardtii*

Cu accumulation by *C. reinhardtii* was determined after 2 and 72 h of exposure to 3.55 nM free $^{65}Cu^{2+}$. The aim was to better characterize the effect of the nutritional status of trace elements in the medium on the accumulation of Cu by *C. reinhardtii*. To this end, two batches of algae were used, differing by the Fe^{3+} level in their growth media: algae acclimated to low-Fe ($[Fe^{3+}]_{free} = 10^{-19}$ M) in the culture medium (L-algae) and algae grown in the culture media containing the replete-Fe ($[Fe^{3+}]_{free} = 10^{-18}$ M) level (M-algae). Both L-algae and M-algae were exposed to $^{65}Cu^{2+}$ under low-Fe and replete-Fe exposure medium. We observed that the amount of Cu accumulated inside L-algae (Figure 1A) was greater when the exposure medium was low in Fe^{3+}, with a concentration of 69 ± 10 amol·cell^{-1} after 2 h of exposure in the low-Fe medium, versus a 9-fold less Cu content of 7.9 ± 0.5 amol·cell^{-1} in replete-Fe medium. This trend was even more marked after 72 h of exposure, reaching 1990 ± 490 amol·cell^{-1} in the low-Fe medium. In comparison, Cu concentrations were 51-fold less in the Fe-replete exposure medium (Figure 1A). For M-algae on the other hand (Figure 1B), the accumulation of $^{65}Cu^{2+}$ after 2 h of exposure was not significantly different when comparing low and replete Fe conditions in the exposure media, and was less than 3 amol·cell^{-1}. This trend remained after 72 h of exposure even as the amount of accumulated Cu increased over time, reaching 77.5 ± 8.1 amol·cell^{-1} in the low-Fe medium, versus 76.4 ± 6.7 amol·cell^{-1} in replete-Fe medium (Figure 1B). This remained much lower than the extent of Cu accumulation by L-algae in low-Fe medium after 72 h (Figure 1A), indicating that Fe^{3+} can influence Cu^{2+} accumulation by the algal cells. Our results show that prolonged exposure of algae in a low-Fe medium makes them more prone to accumulate Cu^{2+}, however, this tendency does appear to be reversible. After 72 h in a replete-Fe exposure medium, Cu^{2+} accumulation by algal cells was reduced by 98% (Figure 1A). This is consistent with our previous work describing the influence of Fe^{3+} on Cu uptake and accumulation in *C. reinhardtii* [7]. In this prior study, we demonstrated over a wide range of low Cu^{2+} concentrations ($10^{-13.0}$ to $10^{-10.5}$ M), that Cu accumulation in *C. reinhardtii* after 72 h increased when low-Fe acclimated cells are exposed in low-Fe conditions, reaching about 150 amol·cell^{-1}. However, Cu levels remained constant over the same range of free Cu^{2+} in a replete-Fe medium [7]. Even if the conditions of the present study are not strictly the same as those of the previous one, the

results obtained in both cases support our hypothesis that Fe^{3+} plays a protective role against Cu^{2+} accumulation and toxicity in *C. reinhardtii*.

Increased accumulation of a given element by algae following their acclimation to low concentrations of this same element is well documented [28, 29], albeit the effect of the homeostatic dynamics of a limiting element (e.g. Fe^{3+}) on that of another element (e.g. Cu^{2+}) is not well known or considered [4]. However, some have reported that this is not always the case for both freshwater [4-6] and marine phytoplankton [30-32]. Given the close link between Fe and Cu metabolism [33-35], we hypothesize that both elements share some common transport systems. This could explain the effect of Fe^{3+} on the accumulation of Cu^{2+} by *C. reinhardtii*, by integrating both the competitive effect between these two elements and the positive feedback in response to a low Fe^{3+} medium [28, 36]. Furthermore, Cu content of L-algae may increase because of the abundance of multicopper oxidase like ferroxidase FOX1 known to be involved in Fe uptake and containing about six Cu per molecule [37, 38]. Furthermore, Cu accumulation under a low-Fe medium by *C. reinhardtii* could result from the use of the same transport system, as observed in marine algae [39, 40]. However, these results on Cu accumulation by algal cells raised questions that deserved further investigations.

3.2 Cu subcellular distribution

The intracellular fate of Cu in *C. reinhardtii* was investigated to understand the internal distribution of this element and the influence of low- versus replete-Fe exposure media on this intracellular fate. To do this, examination of the subcellular distribution of ^{65}Cu was carried out and the presence of Cu detected in four operationally defined subcellular fractions; ORG, GR, HSP and HDP. The ORG and the HDP fractions are categorized as metal-sensitive fractions (since they contain cellular components, such as mitochondria, chloroplast, enzymes and other proteins, for which the biological functions can be sensitive to metal stress) while the HSP and the GR as biologically detoxified metal [27, 41]. After 2 h of exposure, the Cu content in each fraction of L-algae was less than 15 amol·cell^{-1}, regardless of the exposure conditions. Indeed, no fraction contained relatively more than 50% of the total cellular Cu (Figure 2). After 72 h of exposure, the Cu distribution among fractions became markedly different between Fe treatments carried out, indicating both an

effect of Fe^{3+} and a temporal evolution of Cu distribution within cellular compartments. The Cu content of most fractions remained under 30 amol·cell^{-1} when L-algae were exposed to Cu^{2+} in the replete-Fe medium. However, in the low-Fe exposure medium, Cu content reached values of 350 ± 130 amol·cell^{-1} in HSP and 1320 ± 280 amol·cell^{-1} in ORG, i.e. 21% and 78% of the total intracellular Cu, respectively (Figure 2). Thus, after 72 h of exposure as above, Cu distribution in algal cells was as follows: ORG (78 ± 16%) > HSP (20.7 ± 7.8%) > GR (1.16 ± 0.09%) > HDP (< 1%), indicating that approximately 80% of intracellular Cu was in sensitive fractions (dominated by ORG) and the remaining 20% was considered detoxified and mostly stored in dissolved organic forms (HSP). Moreover, and regardless of the exposure media tested, we noticed that between 2 and 72 h of exposure, the proportion of Cu in the ORG fraction increased, and this tendency seems more marked when L-algae were exposed to Cu^{2+} in the low-Fe medium. Indeed, the proportion of Cu in ORG increased from 34.2% after 2 h to 77.6% after 72 h, while it remained between 20.7% and 37.2% in the HSP fraction and decreased in the GR and the HDP fractions (Figure 2B).

In M-algae, the Cu content in the fractions remained low compared to L-algae (Figure 3). Also, no marked differences between treatments were observed. Between 2 and 72 h of exposure to Cu^{2+} the Cu content within fractions increased, with exception of HDP in Fe-replete exposure media (Figure 3A, C), but the proportions in metal sensitive (ORG+HDP) and biologically detoxified metal (HSP+GR) fractions remained globally stable around 50% regardless of the exposure medium (Figure 3B, D). We also noticed that Cu accumulation seemed to increase over time in the ORG fraction. However, even if this proportion reached up to ~60% of the total Cu, the extent of Cu accumulation in M-algae was much lower compared to L-algae (Figure 2B).

Overall, our results show that the intracellular distribution of Cu in *C. reinhardtii* cellular compartments is not constant. This is likely related to the essentiality of this element, the intrinsic function of each cellular compartment and especially the Fe^{3+} nutrient status of the culture and exposure medium. Cu plays a key role in the cell and was found in all cell compartments due to its involvement in electron transfers within the main organelles (ORG), by acting as an enzymatic cofactor (HDP) and the storing of Cu in its detoxified

forms (HSP and GR). Many Cu active sites in various parts of cells were described by [42], and the few available studies also indicated the presence of Cu in subcellular fractions of algae, emphasizing the interspecific character of this distribution [13, 15, 43]. However, no studies have evaluated the role of Fe in this distribution. Indeed, Fe and Cu metabolism is well characterized and well known to be interrelated in microalgae [10, 33, 44], but the homeostatic effects of one on the other have not been elucidated at the subcellular level. However, in other species, previous work has explored the effect of Cu on Fe metabolism and *vice versa* [9, 45, 46]. It is clear from our results that Cu subcellular distribution is strongly altered when the algae are grown under low-Fe conditions. Typically, in the low Cu exposure concentrations ($[^{65}Cu^{2+}]_{free}$ = 3.55 nM), data show that in parallel to Cu detoxification, the Cu requirement of organelles is increasing. Similar Cu hyper-accumulation in *C. reinhardtii* was previously observed within the organelle fraction during Zn-limitation [47]. Cu trafficking to these organelles may be a cell strategy to prevent protein mismetallation during Zn deficiency, enabling efficient cuproprotein metallation or remetallation upon Zn resupply [47]. Our result suggests that Cu may be needed within organelles likely to replace or to fill, directly or indirectly, the Fe deficiency. This substitution phenomenon, well-known in several species of algae including *C. reinhardtii*, usually happens in the opposite manner, with Fe replacing Cu during Cu deficiency [12, 48]. Indeed, to cope with Cu^{2+} deficiency, algae operate a form of Cu economy by reducing essential needs of this element and by promoting the activity of non-Cu-dependent proteins capable of ensuring the same functions. This is the case of plastocyanin, a cuproprotein of the photosynthetic system, replaced by cytochrome c_6 (Cyt c_6) under Cu^{2+} deficiency, and also the case of a Cu amine oxidase replaced by an amine oxidase containing flavin [8, 13, 49]. However, the use of cuproproteins to cope with Fe deficiency conditions in freshwater algae is not reported in the literature. But in marine diatoms continuously exposed to a low-Fe environment, a similar process was documented by [8] resulting from a selective trade-off particularly for the benefit of plastocyanins (the main cuproprotein of chloroplasts). Thus the large number of cellular functions that *C. reinhardtii* tries to keep active when coping with Fe deficiency [50] requires further investigations to allow for a better understanding of our results. This may involve, for instance, characterizing and comparing the entire Cu and Fe transport systems in *C.*

reinhardtii at the molecular level, especially under low-Fe conditions. Therefore, all this implies that cellular metal homeostasis is more complicated than having just detoxification responses; but rather the cell is trying to optimize its metal distribution to maintain growth or vital functions in order to face environmental changes. However, taking into account the entire element economy in a cell, additional research should address this question by looking not only at membrane transporters, but also inside the cell, as elegantly revealed by [15] in their review on Cu homeostasis in algae. In the meantime, it is important to characterize the nature of the Cu-ligand complexes contained in the HSP fraction.

3.3 Potential Cu-binding ligands in the HSP fraction

Microalgae possess a range of potential cellular mechanisms that may be involved in the detoxification of metals [51]. In algal cells, HSP is a fraction that contains biomolecules or bioligands known for their ability to bind metal cations, thus participating in their storage and detoxification. These include certain proteins of the metalloprotein class (e.g. metallochaperones), certain peptides such as GSH and PCs, and amino acids such as cysteine (Cys) [52-54]. Figure 4 shows results of the SEC-ICP-MS and MS/MS analyses performed to characterize the ^{65}Cu signal in the HSP fraction from L-algae after 72 h of exposure to ^{65}Cu ($[^{65}Cu^{2+}]_{free}$ = 39.3 nM) under replete-Fe medium (Figure 4A). The aim was to screen for the biomolecules (peptides, polypeptides, and proteins) contained in this cellular compartment (HSP). In total, we observed six peaks at the following retention times (RT) 11.0 (SEC Peak1: $^{65}Cu_{11.0}$), 13.0 (SEC Peak 2: $^{65}Cu_{13.0}$), 15.04 (SEC Peak 3: $^{65}Cu_{15.04}$), 21.09 (SEC Peak 4: $^{65}Cu_{21.09}$), 29.36 (SEC Peak 5: $^{65}Cu_{29.36}$) and 33.93 (SEC Peak 6: $^{65}Cu_{33.93}$), corresponding to the signal of the ^{65}Cu-biomolecule complexes of different MW contained in the HSP fractions. These complexes can be classified into three operational groups based on their MW, namely (*i*) biomolecules of high molecular weight (HMW; > 15.6 – 7.2 kDa; RT: 10.0 – 17.0 min), (*ii*) biomolecules of medium molecular weight (MMW; 7.2 –< 2.6 kDa; RT: 17.0 – 21.5 min) and (*iii*) those of low molecular weights (LMW; < 2.6 kDa; RT: > 21.5 min). Based on the calibration curve of the chromatographic column, the RT of phytochelatins (PCs) are expected to be found between 22 and 36 min depending on their MW and the chelated cations, which well corresponds to the range of LMW sizes.

To better identify and characterize all potential Cu-bioligands in this cellular compartment, LC-MS/MS analysis was performed on the fractions isolated from SEC. Figure 4B and C, Tables 2, S4 and S5 (Supplementary Material) summarize the essential findings from these experiments. LC-MS/MS analyses (non-targeted proteomics and targeted peptide analyses) were performed to assign the molecular nature of each of the six peaks of the Cu-ligand complexes observed (Figure 4B, C; Tables S4 and S5; Supplementary Material). In Figure 4A, the first SEC Peak ($^{65}Cu_{11.0}$) showed no proteins found from *C. reinhardtii* HSP (only contaminants found with complete uniprot database search) and could correspond to non-specifically bound polymers likely released from the column. The other peaks represent Cu-complexes corresponding to proteins and polypeptides. Proteins (in red) were detected in SEC Peak 2 ($^{65}Cu_{13.0}$) and 3 ($^{65}Cu_{15.04}$). Twenty-one proteins were identified from SEC Peak 2 and six from Peak 3 (with two proteins in common between the two SEC fractions) i.e. a total of 25 proteins identified. Note here that, by using non-targeted proteomic analysis, we wanted to identify as many proteins as possible, so depending on the proteome depth we may miss certain metalloproteins (possibly less abundant than other proteins) in a fraction. Some peptides (PCs and GSH, in green) were detected in SEC fractions 4 to 6. Four different PCs (PC2, 3, 4 and 5) could be confirmed in SEC Peaks 3, 4, 5 and 6 (Figure 4B, C and Table S4; Supplementary Material), based on accurate mass measurements, relative RT and comparison with PC2 and PC6 standard compounds. The presence of GSH (Figure 4B), another important LMW-thiol, was also confirmed by accurate mass and retention time matching with standard GSH. Reduced GSH represents the molecular building block for the biosynthesis of PCs and plays a key role in metal sequestration and in reducing intracellular oxidative stress [51, 55, 56]. These ligands are well known to complex metal ions, including Cu^{2+} [17, 57], however, this is not the case for all 25 proteins detected in Peaks 2 and 3 (see Tables 2 and S5), and their presence in HSP does not necessarily mean that they all bind Cu. Certain proteins listed *a priori* play a role: (*i*) direct or indirect (superoxide dismutase, Calreticulin, Histone H1, 4) in handling Cu detoxification (or another trace element), (*ii*) others because they can alleviate intracellular oxidative stress (Peroxiredoxin, Superoxide dismutase), and (*iii*) others by operational or technical default because they are known for their homeostatic (e.g. Plastocyanin, Acyl carrier protein, carbonic anhydrase, Dihydrolipoyl dehydrogenase) and metabolic (e.g.

carbonic anhydrase, dehydrogenases, 6,7-dimethyl-8-ribityllumazine synthase, etc.) roles. These proteins can overlap on several functions which makes them likely candidates for complexing Cu^{2+}. Only one of these proteins, plastocyanin, is well known to have an active Cu-binding site [15], and another, glyceraldehyde-3-phosphate dehydrogenase, is cited in the literature as having an ability to bind Cu^{2+} [58]. However, carbonic anhydrase has been artificially designed to bind Cu^{2+} and used as a fluorescent probe to monitor cytoplasmic Cu^{2+} [59-61]. Moreover, based on the gene ontology annotation, in addition to carbonic anhydrase and plastocyanin which have active metal sites (Zn^{2+} and Cu^{2+}, respectively), five other proteins in the list would have putative active sites for complexing metals and therefore constitute candidates for Cu-binding ligands in HSP: two superoxide dismutases (AN: A8IGH1(+1) and A8I2E0(+1)), a predicted protein (AN: A8HND3), calmodulin and calreticulin (see details in Table S5).

To identify candidates capable of binding Cu, it is important to define scientifically relevant criteria. Ligands that can form stable complexes with metals include S-, N-/O-, and O-containing functional groups [57, 62]. However, it is known that in biological systems the situation is much more complex and metal concentrations in cells is often changing, based for instance on the growth conditions [57, 63]. First, Cu-containing proteins were organized into three groups based on their nuclearity, Electron Paramagnetic Resonance (EPR) and UV-visible spectroscopic characteristics, and common amino-acid side chains [62]. Based on this, [64] first proposed three different types of protein-bound Cu, usually referred to as Types 1 to 3. Even though this categorization and terminology is still widely-used today, it should be noted that our knowledge of Cu biochemistry has improved since then and now includes many Cu species that do not fit within these parameters [62, 65]. Therefore, our first criterion to identify good Cu-binding candidate proteins was the number of Cys residues in the protein. Given the important role played by Cys within protein and peptide metal binding sites [62, 66], it is possible to define for each protein a Cys-to-protein (in total amino acid residues) ratio (Table S5). Based on the threshold of x% of Cys (arbitrarily fixed) we can define good candidate proteins as those having a ratio higher than the fixed threshold. Thus, for a threshold of 2%, only three proteins (carbonic anhydrase, CP12 domain-containing protein and one predicted protein (AN: A8HND3)) are candidates in the list of 25 proteins, i.e. around 13%, of which two are clearly annotated as being able to

bind metals (Table S5). Among these two proteins, only carbonic anhydrase is known to have the ability to bind Cu [59, 61] but no clear evidence is established as to its role in Cu detoxification. The second protein (AN: A8HND3) is a predicted and annotated protein that can bind metal ions but requires further investigations to determine if it also has the ability to bind Cu and be potentially involved in its detoxification. It is also possible to refine this approach by adding or by combining several relevant criteria. For example, by combining the ratios of the seven most frequent or more probable amino acids encountered in the metal-binding sites (Arg, His, Lys, Cys, Met, Asp, Glu) (see Table S5 and [62]) and we can deduce a classification score for each protein in decreasing order of plausible candidates for complexing Cu. While relevant, the latter approach requires even further investigations to achieve the most realistic combination. A similar method based on score calculations was used by [67]. Another approach may consist of the use of bioinformatic tools to search for patterns (or protein profiles) that are conserved and characteristic of the binding sites of divalent metals, in particular Cu [68-70]. These motifs can not only suggest putative functions of uncharacterized proteins, but also on their possible metal cofactors [70-72]. Cu-binding motifs have been identified and characterized in many proteins. The amino-terminal Cu(II)- and Ni(II)-binding (ATCUN) motif, is an example of a Cu(II)-binding motif that shows high affinity and specificity for Cu(II) (or Ni(II)), and well known for its ability to facilitate metal exchange with appropriate receptor ligands [71, 73]. The way in which Cu is coordinated by these motifs is therefore important for its intracellular distribution and also for effective functioning of Cu-dependent proteins. Indeed, based on the conservation of these motifs, [67] built a web application that facilitates identification of binding sites (for 12 metal ions) that may exist on a protein sequence listed in the Protein Data Bank (PDB). But using this server requires, among other things, knowledge of the PDB ID of the protein of interest and its sequence must not have more than 1000 residues. When these two requirements were met for our proteins (i.e. 4 out of 25), the results always indicated several Cu-binding sites. It is thus likely that the other proteins also have Cu-binding sites, which would explain their presence in the HSP fraction. It would be interesting to use other hyphenated techniques that combine a high resolution separation technique, like gel or capillary electrophoresis, with sensitive elemental (ICP) or molecular (electrospray ionization or matrix-assisted laser desorption/ionization) mass spectrometric

detection to better characterize the Cu-protein complexes detected [74, 75]. In addition, the combined use of X-ray crystallography and mass spectrometry could also be a valuable strategy to investigate and characterize metal binding sites in proteins [76, 77].

4. Conclusion

Cu is an essential element and its homeostasis is tightly and efficiently regulated. However, this capacity to keep the internal Cu concentration within an optimal range can sometimes be disturbed. Our results show that an Fe^{3+}-depleted medium disrupts Cu homeostasis in algal cells, which greatly increased the extent of Cu accumulation. The freshwater green alga *C. reinhardtii* can cope with this by mobilizing various internal mechanisms to manage the excess Cu. In accordance with our hypothesis, we found that these mechanisms involved the binding of metals through bioligands like GSH and PCs. In addition to these LMWs ligands, we detected in the HSP fraction many proteins, categorized as MMW and HMW ligands, but the effective role of most of them in the Cu detoxification process in *C. reinhardtii* remains unknown. We have also highlighted another strategy used by algae in low-Fe conditions in which organelles are highly involved. We hypothesize that this Cu traffic to organelles could be in response to the Fe deficit by replacing Fe with Cu, in particular to maintain vital functions like respiration (or photosynthesis) through electron transfer chains as reported in marine diatoms. These results shed new light on the adaptive capacities of *C. reinhardtii*, which is a model organism encountered over several latitudes, to cope with wide environment physicochemical variations. A molecular characterization (metallomics, proteomics and metabolomics) of the ORG fraction could further shed light on these mechanisms. Our results could also have physiological links with changes in membrane transporters related to the Fe nutritional context of the medium. Therefore, to better understand these results, further study of the mechanisms governing the internalization of Cu and Fe in algae will be important.

Conflicts of interest

Authors have no conflicts to declare.

Acknowledgements

The authors acknowledge the technical assistance provided by J. Perreault, O. Hourtané, N. Dupuy and K. Racine. Language assistance provided by S. Hepditch is also gratefully acknowledged. Valuable comments provided by C. Guéguen and M.R. Twiss helped improve the manuscript.

Funding

This work was supported by EcotoQ (FRQNT strategic network grant; 2020-RS4-265031), by the Natural Sciences and Engineering Research Council (NSERC Discovery Grant; RGPIN-2014-05082), and the Canada Research Chair program (950-231107).

Data availability satatement

The data underlying this article are available in Dataverse, at https://doi.org/10.5683/SP3/TPCDLZ.

Author contributions

These results were part of the PhD thesis of Emeric Kochoni who conducted all experiments. The subcellular fractionation and SEC-ICP-MS measurements were performed by Dr. Kochoni in collaboration with Dr. Imad Aharchaou. All metal measurements, data treatment as well as manuscript drafting were done by Dr. Kochoni. LC-MS/MS analyses were conducted by Ms. Leanne Ohlund, under the supervision of Prof. Lekha Sleno. Prof. Maikel Rosabal was involved in the conception of the metallomics and proteomics experiments with Prof. Sleno. Prof. Claude Fortin was the principal investigator in charge of funding, conceptualization of the work and overall supervision. All authors contributed to data analysis and manuscript writing.

5 References

1. Brix KV, Tellis MS, Crémazy A *et al.* Characterization of the effects of binary metal mixtures on short-term uptake of Cd, Pb, and Zn by rainbow trout (*Oncorhynchus mykiss*). *Aquat Toxicol* 2017;**193**:217-27. doi: 10.1016/j.aquatox.2017.10.015
2. Adams W, Blust R, Dwyer R *et al.* Bioavailability assessment of metals in freshwater environments: A historical review. *Environ Toxicol Chem* 2020;**39**(1):48-59. doi: 10.1002/etc.4558
3. Mebane CA, Chowdhury MJ, De Schamphelaere KAC *et al.* Metal bioavailability models: Current status, lessons learned, considerations for regulatory use, and the path forward. *Environ Toxicol Chem* 2020;**39**(1):60-84. doi: 10.1002/etc.4560
4. Lavoie M, Fortin C, Campbell PGC. Influence of essential elements on cadmium uptake and toxicity in a unicellular green alga: The protective effect of trace zinc and cobalt concentrations. *Environ Toxicol Chem* 2012;**31**(7):1445-52. doi: 10.1002/etc.1855
5. Töpperwien S, Behra R, Sigg L. Competition among zinc, manganese, and cadmium uptake in the freshwater alga *Scenedesmus vacuolatus*. *Environ Toxicol Chem* 2007;**26**(3):483-90. doi: 10.1897/06-181R.1
6. Sunda WG, Huntsman SA. Interactions among Cu^{2+}, Zn^{2+}, and Mn^{2+} in controlling cellular Mn, Zn, and growth rate in the coastal alga *Chlamydomonas*. *Limnol Oceanogr* 1998;**43**(6):1055-64. doi: 10.4319/lo.1998.43.6.1055
7. Kochoni E, Fortin C. Iron modulation of copper uptake and toxicity in a green alga (*Chlamydomonas reinhardtii*). *Environ Sci Technol* 2019;**53**(11):6539-45. doi: 10.1021/acs.est.9b01369
8. Schoffman H, Lis H, Shaked Y *et al.* Iron–nutrient interactions within phytoplankton. *Front Plant Sci* 2016;**7**:1223. doi: 10.3389/fpls.2016.01223
9. Maldonado MT, Allen AE, Chong JS *et al.* Copper-dependent iron transport in coastal and oceanic diatoms. *Limnol Oceanogr* 2006;**51**(4):1729–43. doi: 10.4319/lo.2006.51.4.1729
10. Blaby-Haas CE, Merchant SS. The ins and outs of algal metal transport. *Biochim Biophys Acta* 2012;**1823**(9):1531-52. doi: 10.1016/j.bbamcr.2012.04.010
11. Glaesener AG, Merchant SS, Blaby-Haas CE. Iron economy in *Chlamydomonas reinhardtii*. *Front Plant Sci* 2013;**4**(337):1-12. doi: 10.3389/fpls.2013.00337
12. Hanikenne M, Merchant SS, Hamel P. Transition metal nutrition: A balance between deficiency and toxicity. In: Stern DB, Witman GBs (eds). *The Chlamydomonas Sourcebook: Organellar and Metabolic Processes*. London: Academic Press, 2009, 333-99
13. Kropat J, Gallaher SD, Urzica EI *et al.* Copper economy in *Chlamydomonas*: Prioritized allocation and reallocation of copper to respiration vs. photosynthesis. *Proc Natl Acad Sci USA* 2015;**112**(9):2644-51. doi: 10.1073/pnas.1422492112
14. Merchant SS, Allen MD, Kropat J *et al.* Between a rock and a hard place: Trace element nutrition in *Chlamydomonas*. *Biochim Biophys Acta* 2006;**1763**(7):578-94. doi: 10.1016/j.bbamcr.2006.04.007
15. Merchant SS, Schmollinger S, Strenkert D *et al.* From economy to luxury: Copper homeostasis in *Chlamydomonas* and other algae. *Biochim Biophys Acta* 2020;**1867**(11):118822. doi: 10.1016/j.bbamcr.2020.118822

16. Cobbett CS. Phytochelatins and their roles in heavy metal detoxification. *Plant Physiol* 2000;**123**(3):825-32. doi: 10.1104/pp.123.3.825
17. Navarrete A, González A, Gómez M *et al.* Copper excess detoxification is mediated by a coordinated and complementary induction of glutathione, phytochelatins and metallothioneins in the green seaweed Ulva compressa. *Plant Physiol Biochem* 2018. doi: https://doi.org/10.1016/j.plaphy.2018.11.019
18. Crémazy A, Levy JL, Campbell PGC *et al.* Uptake and subcellular partitioning of trivalent metals in a green alga: Comparison between Al and Sc. *BioMetals* 2013;**26**(6):989-1001. doi: 10.1007/s10534-013-9675-6
19. Lavoie M, Le Faucheur S, Fortin C *et al.* Cadmium detoxification strategies in two phytoplankton species: Metal binding by newly synthesized thiolated peptides and metal sequestration in granules. *Aquat Toxicol* 2009;**92**(2):65-75. doi: 10.1016/j.aquatox.2008.12.007
20. Haraguchi H. Metallomics: The history over the last decade and a future outlook. *Metallomics* 2017;**9**(8):1001-13. doi: 10.1039/C7MT00023E
21. Haraguchi H, Ishii A, Hasegawa T *et al.* Metallomics study on all-elements analysis of salmon egg cells and fractionation analysis of metals in cell cytoplasm. *Pure Appl Chem* 2008;**80**(12):2595-608. doi: 10.1351/pac200880122595
22. Pérez-Pérez ME, Mauriès A, Maes A *et al.* The deep thioredoxome in *Chlamydomonas reinhardtii:* New insights into redox regulation. *Mol Plant* 2017;**10**(8):1107-25. doi: 10.1016/j.molp.2017.07.009
23. Hassler C, Slaveykova V, Wilkinson K. Discriminating between intra-and extracellular metals using chemical extractions. *Limnol Oceanogr Methods* 2004;**2**(7):237 - 47. doi: 10.4319/lom.2004.2.237
24. Lavoie M, Bernier J, Fortin C *et al.* Cell homogenization and subcellular fractionation in two phytoplanktonic algae: Implications for the assessment of metal subcellular distributions. *Limnol Oceanogr Methods* 2009;**7**(4):277-86. doi: 10.4319/lom.2009.7.277
25. Campbell PGC, Giguère A, Bonneris E *et al.* Cadmium-handling strategies in two chronically exposed indigenous freshwater organisms—the yellow perch (*Perca flavescens*) and the floater mollusc (*Pyganodon grandis*). *Aquat Toxicol* 2005;**72**(1):83-97. doi: 10.1016/j.aquatox.2004.11.023
26. Cardon P-Y, Triffault-Bouchet G, Caron A *et al.* Toxicity and Subcellular Fractionation of Yttrium in Three Freshwater Organisms: Daphnia magna, Chironomus riparius, and Oncorhynchus mykiss. *ACS Omega* 2019;**4**(9):13747-55. doi: 10.1021/acsomega.9b01238
27. Aharchaou I, Rosabal M, Liu F *et al.* Bioaccumulation and subcellular partitioning of Cr(III) and Cr(VI) in the freshwater green alga *Chlamydomonas reinhardtii*. *Aquat Toxicol* 2017;**182**:49-57. doi: http://dx.doi.org/10.1016/j.aquatox.2016.11.004
28. Lavoie M, Campbell P, Fortin C. Importance de mieux connaître les mécanismes de transport des métaux pour la prédiction de l'accumulation et de la toxicité des métaux dissous chez le phytoplancton : Récentes avancées et défis pour le développement du modèle du ligand biotique. *Rev Sci l'Eau* 2016;**29**(2):119-47. doi: 10.7202/1036544ar
29. Bossuyt BTA, Janssen CR. Long-term acclimation of *Pseudokirchneriella subcapitata* (Korshikov) Hindak to different copper concentrations: changes in tolerance and physiology. *Aquat Toxicol* 2004;**68**(1):61-74. doi: 10.1016/j.aquatox.2004.02.005

30. Annett AL, Lapi S, Ruth TJ *et al.* The effects of Cu and Fe availability on the growth and Cu:C ratios of marine diatoms. *Limnol Oceanogr* 2008;**53**(6):2451-61. doi: 10.4319/lo.2008.53.6.2451
31. Guo J, Annett AL, Taylor RL *et al.* Copper-uptake kinetics of coastal and oceanic diatoms. *J Phycol* 2010;**46**(6):1218-28. doi: 10.1111/j.1529-8817.2010.00911.x
32. Peers G, Quesnel S-A, Price NM. Copper requirements for iron acquisition and growth of coastal and oceanic diatoms. *Limnol Oceanogr* 2005;**50**(4):1149-58. doi: 10.4319/lo.2005.50.4.1149
33. La Fontaine S, Quinn J, Merchant S. Comparative analysis of copper and iron metabolism in photosynthetic eukaryotes vs yeast and mammals. In: E.J. Massaro (ed). *Handbook of Copper Pharmacology and Toxicology*. Totowa, NJ.: Springer, Humana Press, 2002, 481-502
34. Arredondo M, Núñez MT. Iron and copper metabolism. *Mol Asp Med* 2005;**26**(4):313-27. doi: 10.1016/j.mam.2005.07.010
35. Taylor AB, Stoj CS, Ziegler L *et al.* The copper-iron connection in biology: Structure of the metallo-oxidase Fet3p. *Proc Natl Acad Sci USA* 2005;**102**(43):15459-64. doi: 10.1073/pnas.0506227102
36. Raven JA. Nutrient transport in microalgae. In: Rose AH, Morris JG (eds). *Adv Microb Physiol*. New York, NY, U.S.A.: Academic Press, 1981, 47-226
37. Chen J-C, Hsieh SI, Kropat J *et al.* A ferroxidase encoded by FOX1 contributes to iron assimilation under conditions of poor iron nutrition in *Chlamydomonas*. *Eukaryot Cell* 2008;**7**(3):541-5. doi: 10.1128/EC.00463-07
38. La Fontaine S, Quinn JM, Nakamoto SS *et al.* Copper-dependent iron assimilation pathway in the model photosynthetic eukaryote *Chlamydomonas reinhardtii*. *Eukaryot Cell* 2002;**1**(5):736-57. doi: 10.1128/EC.1.5.736-757.2002
39. Lane ES, Jang K, Cullen JT *et al.* The interaction between inorganic iron and cadmium uptake in the marine diatom *Thalassiosira oceanica*. *Limnol Oceanogr* 2008;**53**(5):1784-9. doi: 10.4319/lo.2008.53.5.1784
40. Lane ES, Semeniuk DM, Strzepek RF *et al.* Effects of iron limitation on intracellular cadmium of cultured phytoplankton: Implications for surface dissolved cadmium to phosphate ratios. *Mar Chem* 2009;**115**(3–4):155-62. doi: 10.1016/j.marchem.2009.07.008
41. Wallace WG, Lee B-G, Luoma SN. Subcellular compartmentalization of Cd and Zn in two bivalves. I. Significance of metal-sensitive fractions (MSF) and biologically detoxified metal (BDM). *Mar Ecol Prog Ser* 2003;**249**:183-97. doi: 10.3354/meps249183
42. Solomon EI, Heppner DE, Johnston EM *et al.* Copper active sites in biology. *Chem Rev* 2014;**114**(7):3659-853. doi: 10.1021/cr400327t
43. Morelli E, Scarano G. Copper-induced changes of non-protein thiols and antioxidant enzymes in the marine microalga *Phaeodactylum tricornutum*. *Plant Sci* 2004;**167**(2):289-96. doi: 10.1016/j.plantsci.2004.04.001
44. Scheiber IF, Pilátová J, Malych R *et al.* Copper and iron metabolism in *Ostreococcus tauri* – the role of phytotransferrin, plastocyanin and a chloroplast copper-transporting ATPase. *Metallomics* 2019;**11**(10):1657-66. doi: 10.1039/C9MT00078J
45. Gulec S, Collins JF. Molecular mediators governing iron-copper interactions. *Annu Rev Nutr* 2014;**34**:95-116. doi: 10.1146/annurev-nutr-071812-161215

46. Semeniuk DM, Taylor RL, Bundy RM *et al.* Iron–copper interactions in iron-limited phytoplankton in the northeast subarctic Pacific Ocean. *Limnol Oceanogr* 2016;**61**(1):279-97. doi: doi:10.1002/lno.10210
47. Hong-Hermesdorf A, Miethke M, Gallaher SD *et al.* Subcellular metal imaging identifies dynamic sites of Cu accumulation in *Chlamydomonas*. *Nat Chem Biol* 2014;**10**(12):1034-42. doi: 10.1038/nchembio.1662
48. Castruita M, Casero D, Karpowicz SJ *et al.* Systems biology approach in *Chlamydomonas* reveals connections between copper nutrition and multiple metabolic steps. *Plant Cell* 2011;**23**(4):1273-92. doi: 10.1105/tpc.111.084400
49. Hsieh SI, Castruita M, Malasarn D *et al.* The proteome of copper, iron, zinc, and manganese micronutrient deficiency in *Chlamydomonas reinhardtii*. *Mol Cell Proteomics* 2013;**12**(1):65-86. doi: 10.1074/mcp.M112.021840
50. Blaby-Haas CE, Merchant SS. Iron sparing and recycling in a compartmentalized cell. *Curr Opin Microbiol* 2013;**16**(6):677-85. doi: 10.1016/j.mib.2013.07.019
51. Lavoie M, Raven JA, Jones OAH *et al.* Energy cost of intracellular metal and metalloid detoxification in wild-type eukaryotic phytoplankton. *Metallomics* 2016. doi: 10.1039/C6MT00049E
52. Balzano S, Sardo A, Blasio M *et al.* Microalgal metallothioneins and phytochelatins and their potential use in bioremediation. *Front Microbiol* 2020;**11**(517):517-. doi: 10.3389/fmicb.2020.00517
53. Cobbett C, Goldsbrough P. Phytochelatins and metallothioneins: Roles in heavy metal detoxification and homeostasis. *Annu Rev Plant Biol* 2002;**53**(1):159-82. doi: 10.1146/annurev.arplant.53.100301.135154
54. Smith CL, Steele JE, Stauber JL *et al.* Copper-induced changes in intracellular thiols in two marine diatoms: *Phaeodactylum tricornutum* and *Ceratoneis closterium*. *Aquat Toxicol* 2014;**156**:211-20. doi: 10.1016/j.aquatox.2014.08.010
55. Miao A-J, Wang W-X. Predicting copper toxicity with its intracellular or subcellular concentration and the thiol synthesis in a marine diatom. *Environ Sci Technol* 2007;**41**(5):1777-82. doi: 10.1021/es0613963
56. Rauser WE. Phytochelatins and related peptides. Structure, biosynthesis, and function. *Plant Physiol* 1995;**109**(4):1141-9. doi: 10.1104/pp.109.4.1141
57. Seregin IV, Kozhevnikova AD. Low-molecular-weight ligands in plants: Role in metal homeostasis and hyperaccumulation. *Photosynthesis Res* 2020;**145**(1). doi: 10.1007/s11120-020-00768-1
58. Matsumura H, Kai A, Maeda T *et al.* Structure basis for the regulation of glyceraldehyde-3-phosphate dehydrogenase activity via the intrinsically disordered protein CP12. *Structure* 2011;**19**(12):1846-54. doi: 10.1016/j.str.2011.08.016
59. Kim JK, Lee C, Lim SW *et al.* Elucidating the role of metal ions in carbonic anhydrase catalysis. *Nat Commun* 2020;**11**(1):4557. doi: 10.1038/s41467-020-18425-5
60. Tabbì G, Magrì A, Rizzarelli E. The copper(II) binding centres of carbonic anhydrase are differently affected by reductants that ensure the redox intracellular environment. *J Inorg Biochem* 2019;**199**:110759. doi: 10.1016/j.jinorgbio.2019.110759
61. Linder MC. *Biochemistry of copper.* New York: Springer Science & Business Media, 1991
62. Doerrer LH. Cu in biology: Unleashed by O_2 and now irreplaceable. *Inorg Chim Acta* 2018;**481**:4-24. doi: 10.1016/j.ica.2017.11.051

63. Gayomba S, Zhai Z, Jung H-i *et al.* Local and systemic signaling of iron status and its interactions with homeostasis of other essential elements. *Front Plant Sci* 2015;**6**(716). doi: 10.3389/fpls.2015.00716
64. Malkin R, Malmström BG. The state and function of copper in biological systems. *Adv Enzymol Relat Areas Mol Biol* 1970;**33**:177-244. doi: 10.1002/9780470122785.ch4
65. Gray HB, Malmström BG, Williams R. Copper coordination in blue proteins. *J Biol Inorg Chem* 2000;**5**(5):551-9. doi: 10.1007/s007750000146
66. Banci L, Bertini I, Cantini F *et al.* Cellular copper distribution: A mechanistic systems biology approach. *Cell Mol Life Sci* 2010;**67**(15):2563-89. doi: 10.1007/s00018-010-0330-x
67. Lin Y-F, Cheng C-W, Shih C-S *et al.* MIB: Metal ion-binding site prediction and docking server. *J Chem Inf Model* 2016;**56**(12):2287-91. doi: 10.1021/acs.jcim.6b00407
68. Chan ACK, Lin H, Koch D *et al.* A copper site is required for iron transport by the periplasmic proteins P19 and FetP. *Metallomics* 2020;**12**(10):1530-41. doi: 10.1039/D0MT00130A
69. Cobbett CS, Hussain D, Haydon MJ. Structural and functional relationships between type 1B heavy metal-transporting P-type ATPases in *Arabidopsis*. *New Phytol* 2003;**159**(2):315-21. doi: 10.1046/j.1469-8137.2003.00785.x
70. Shin L-J, Lo J-C, Yeh K-C. Copper chaperone antioxidant protein1 is essential for copper homeostasis. *Plant Physiol* 2012;**159**(3):1099-110. doi: 10.1104/pp.112.195974
71. Koch KA, Peña MMO, Thiele DJ. Copper-binding motifs in catalysis, transport, detoxification and signaling. *Chem Biol* 1997;**4**(8):549-60. doi: 10.1016/S1074-5521(97)90241-6
72. Pretzler M, Rompel A. What causes the different functionality in type-III-copper enzymes? A state of the art perspective. *Inorg Chim Acta* 2018;**481**:25-31. doi: 10.1016/j.ica.2017.04.041
73. Neupane KP, Aldous AR, Kritzer JA. Metal-binding and redox properties of substituted linear and cyclic ATCUN motifs. *J Inorg Biochem* 2014;**139**:65-76. doi: 10.1016/j.jinorgbio.2014.06.004
74. Mounicou S, Szpunar J, Lobinski R. Metallomics: The concept and methodology. *Chem Soc Rev* 2009;**38**(4):1119-38. doi: 10.1039/B713633C
75. Bouyssiere B, Lobinski R, Szpunar J. Hyphenated techniques in environmental speciation analysis. *Spectroscopy*, 2003, 391-410
76. Handing KB, Niedzialkowska E, Shabalin IG *et al.* Characterizing metal-binding sites in proteins with X-ray crystallography. *Nat Protoc* 2018;**13**(5):1062-90. doi: 10.1038/nprot.2018.018
77. Messori L, Merlino A. Protein metalation by metal-based drugs: X-ray crystallography and mass spectrometry studies. *Chem Comm* 2017;**53**(85):11622-33. doi: 10.1039/C7CC06442J

Tables and Figures

Table 1: Molecular formula, exact mass information and corresponding retention times (RT) for glutathione (GSH) and phytochelatins (PCs) analyzed by liquid chromatography-high resolution mass spectrometry using two complementary chromatographic columns

Name	**Formula**	**Neutral mass**	**ion**	***m/z***	**Scherzo RT (min)**	**Eclipse RT (min)**
GSH	$C_{10}H_{17}N_3O_6S$	307.0838	-H	306.0765	2.6	
PC2	$C_{18}H_{29}N_5O_{10}S_2$	539.1356	-H	538.1283	7.9	2.4
PC3	$C_{26}H_{41}N_7O_{14}S_3$	771.1874	-2H	384.5864		3.5
PC4	$C_{34}H_{53}N_9O_{18}S_4$	1003.2391	-2H	500.6123		4.2
PC5	$C_{42}H_{65}N_{11}O_{22}S_5$	1235.2909	-2H	616.6382		4.7
PC6	$C_{50}H_{77}N_{13}O_{26}S_6$	1467.3427	-2H	732.6641		5.1

Table 2: Proteins identified in SEC fractions 2 and 3 using bottom-up proteomics LC-MS/MS analysis

SEC Fractions (#)	Accession Number	MW (kDa)	Sequence coverage (%)	# unique peptides	Protein name
2	A8IT01	42	44	21	Carbonic anhydrase
2	Q9FE86	26	41	11	Peroxiredoxin
2	A8HP84	40	26	8	Glyceraldehyde-3-phosphate dehydrogenase
2	A8I2V3	22	54	8	Peroxiredoxin
2	A8IGH1	26	41	9	Superoxide dismutase
2	A8I2E0	24	27	6	Superoxide dismutase
2	A8I8Z1	23	21	4	6,7-dimethyl-8-ribityllumazine synthase
2	A0A2K3DMT2	323	1.6	3	Uncharacterized protein
2	A8J0E4	31	21	6	Oxygen-evolving enhancer protein 1 of photosystem II
2	A0A2K3E5S1	61	9.2	4	Uncharacterized protein
2	Q945T1	28	11	3	GrpE protein homolog
2	A8HSB0	11	29	3	Histone H4
2	A8IDP6	18	20	2	Calmodulin
2	A8J9H8	17	24	3	Nucleoside diphosphate kinase
2	A8HMC0	47	6.9	2	Calreticulin
2	A8HRZ0	27	7.9	2	Histone H1
2	A0A2K3DCZ1	54	4.0	2	Uncharacterized protein
2	A8J1T4	52	4.6	2	Dihydrolipoyl dehydrogenase
2	A8J2X6	41	6.5	2	N-acetyl-glutamate semialdehyde dehydrogenase
2 / 3	A0A2K3DA85	32	2.5 / 19	1 / 5	Uncharacterized protein
2 / 3	Q6UKY5	12	11 / 22	1 / 2	Acyl carrier protein
3	A8JH68	15	28	6	Plastocyanin
3	A0A2K3DI03	14	21	3	CP12 domain-containing protein
3	A8IAW5	16	19	2	Predicted protein
3	A8HND3	11	23	3	Predicted protein

Figures

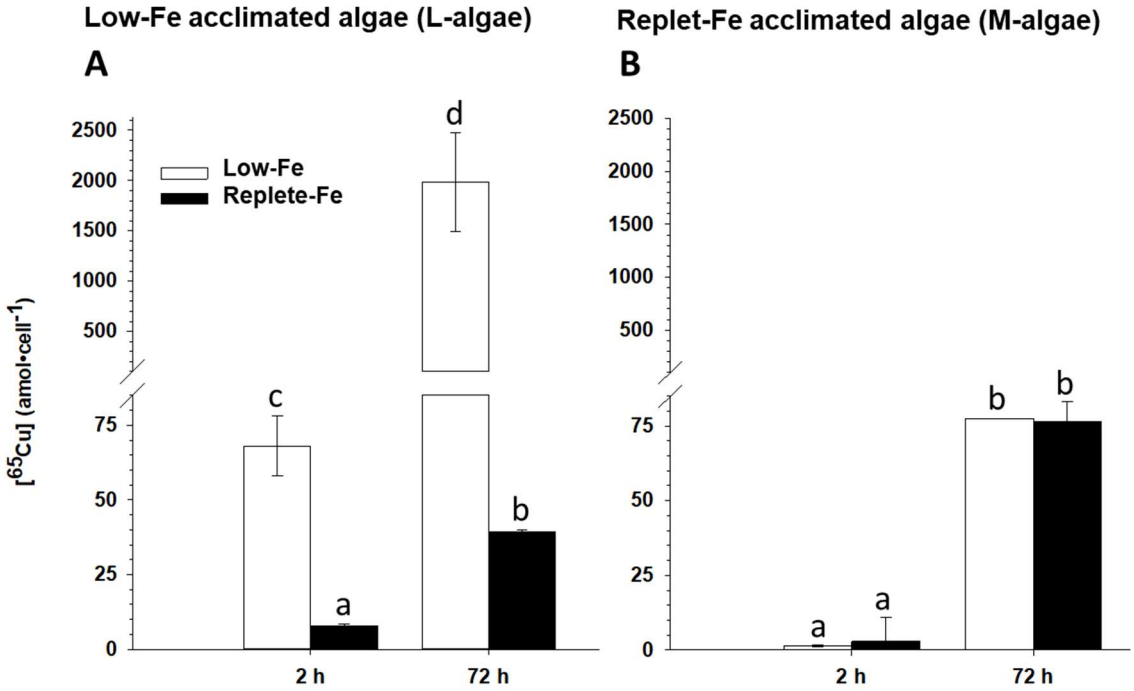

Figure 1: Cu accumulation (amol·cell^{-1}; ±SD, n = 3) by *C. reinhardtii* after 2 and 72 h of exposure to ^{65}Cu ($[^{65}Cu^{2+}]_{free}$ = 3.55 nM) in a low-Fe medium ($[Fe^{3+}]_{free} = 10^{-19}$ M) or a replete-Fe medium ($[Fe^{3+}]_{free} = 10^{-18}$ M). In (A) algal cells were previously grown in a low-Fe medium ($[Fe^{3+}]_{free} = 10^{-19}$ M; acclimated algae or L-algae) and in (B) algal cells were not acclimated to a low-Fe medium ($[Fe^{3+}]_{free} = 10^{-18}$ M; non-acclimated algae or M-algae). Different letters indicate statistically significant differences at $p < 0.05$ (Kruskal-Wallis test followed by Tukey Kramer HSD test).

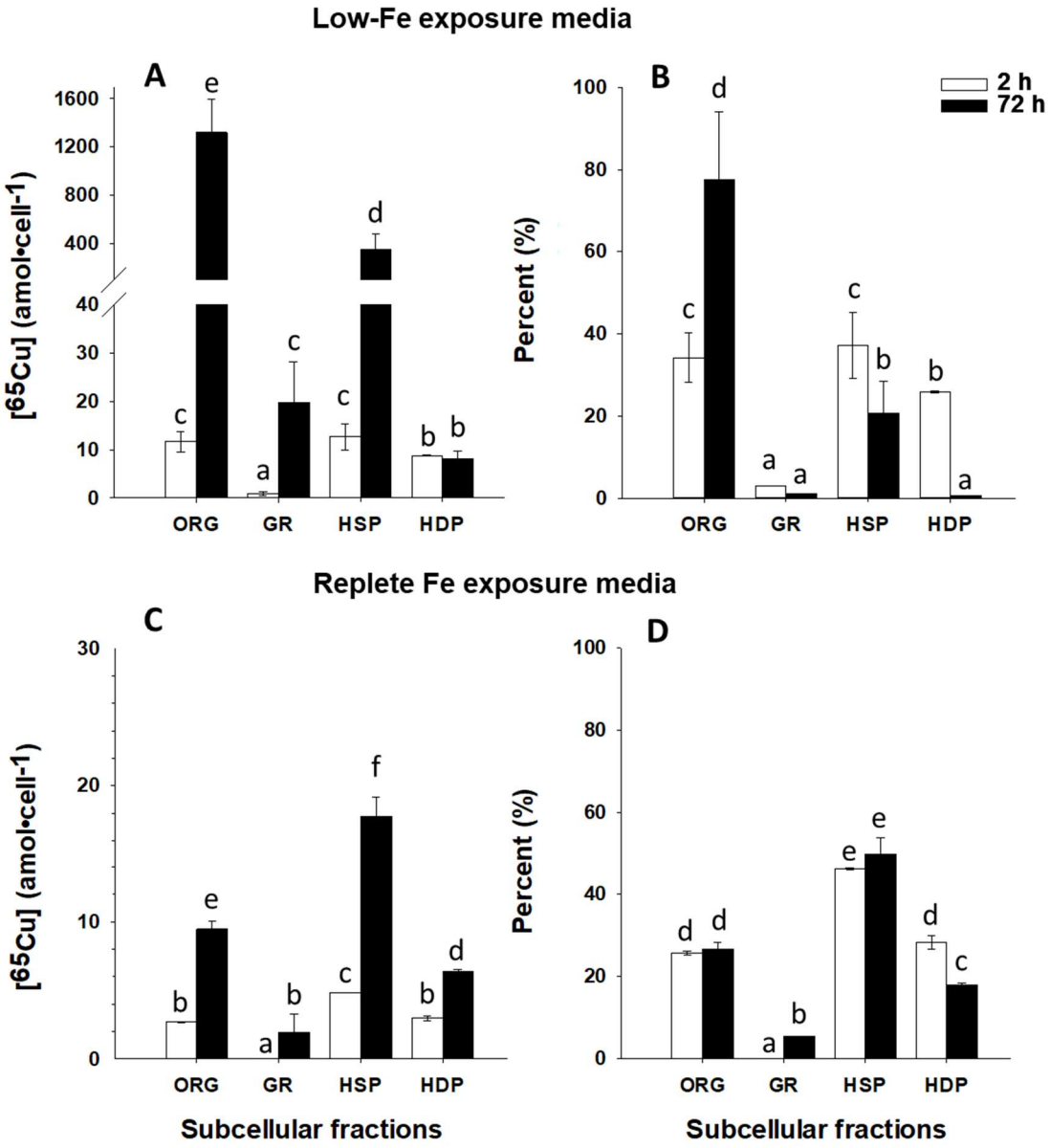

Figure 2: Cu subcellular distribution in *C. reinhardtii* acclimated to low-Fe media (L-algae; $[Fe^{3+}]_{free} = 10^{-19}$ M) and subsequently exposed to $^{65}Cu^{2+}$ ($[^{65}Cu^{2+}]_{free} = 3.55$ nM) for 2 and 72 h in a low-Fe medium ($[Fe^{3+}]_{free} = 10^{-19}$ M, A: Absolute values, B: Relative values) or in a replete-Fe medium ($[Fe^{3+}]_{free} = 10^{-18}$ M, C: Absolute values, D: Relative values). Different letters indicate statistically significant differences at $p < 0.05$ (Kruskal-Wallis test followed by Tukey Kramer HSD test). Error bars are the standard deviations of three replicates (n=3). ORG = organelles; GR = granules; HSP = heat-stable proteins and peptides; and HDP = heat-denatured proteins.

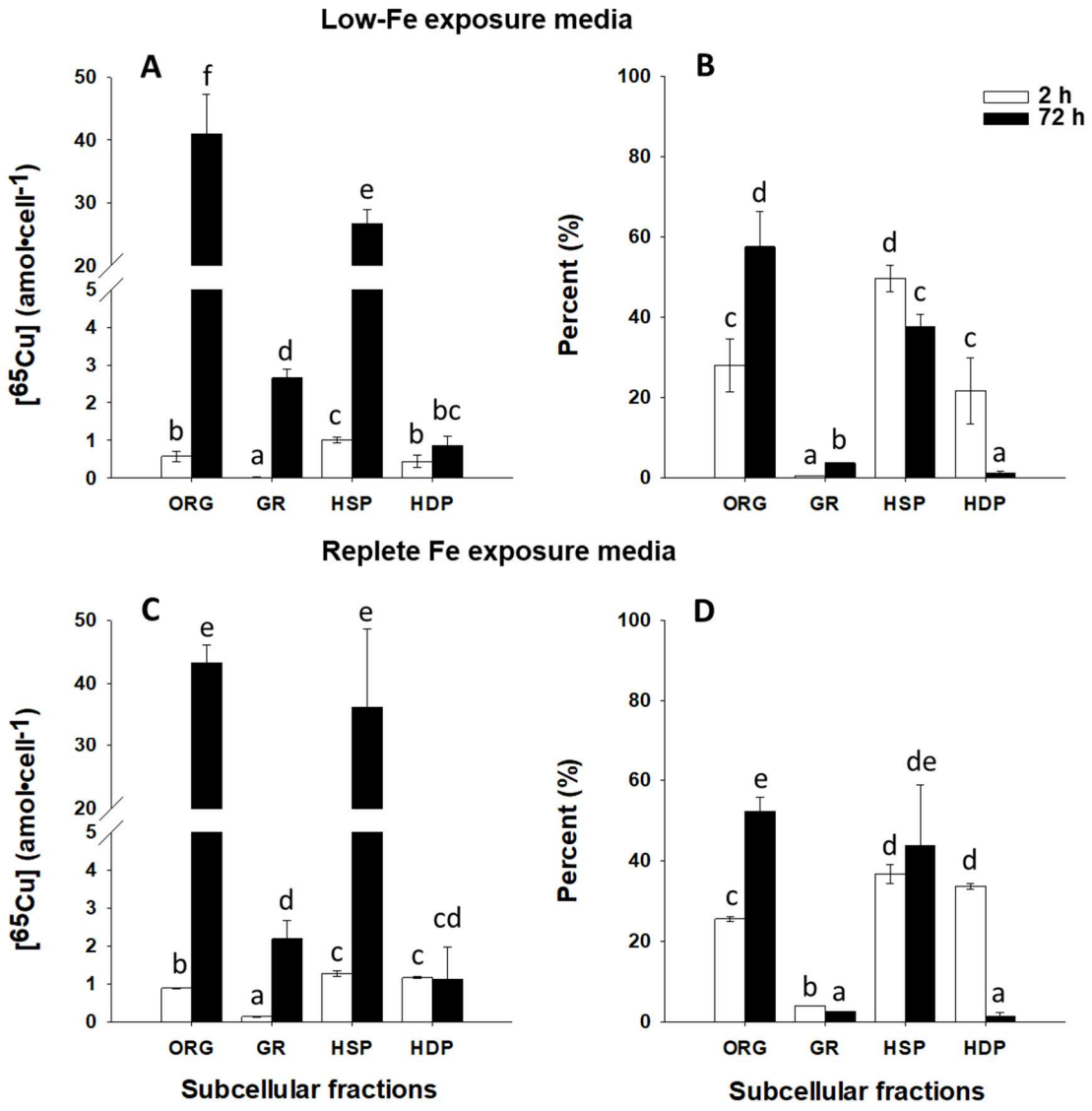

Figure 3: Cu subcellular distribution in *C. reinhardtii* not acclimated to low-Fe media (M-algae; $[Fe^{3+}]_{free}$ = 10^{-18} M) and exposed to $^{65}Cu^{2+}$ ($[^{65}Cu^{2+}]_{free}$ = 3.55 nM) for 2 and 72 h in a low-Fe medium ($[Fe^{3+}]_{free}$ = 10^{-19} M, A: Absolute values, B: Relative values) or in a replete-Fe medium ($[Fe^{3+}]_{free}$ = 10^{-18} M, C: Absolute values, D: Relative values). Different letters indicate statistically significant differences at $p < 0.05$ (Kruskal-Wallis test followed by Tukey Kramer HSD test). Error bars are the standard deviations of three replicates (n=3). ORG = organelles; GR = granules; HSP = heat-stable proteins and peptides; and HDP = heat-denatured proteins.

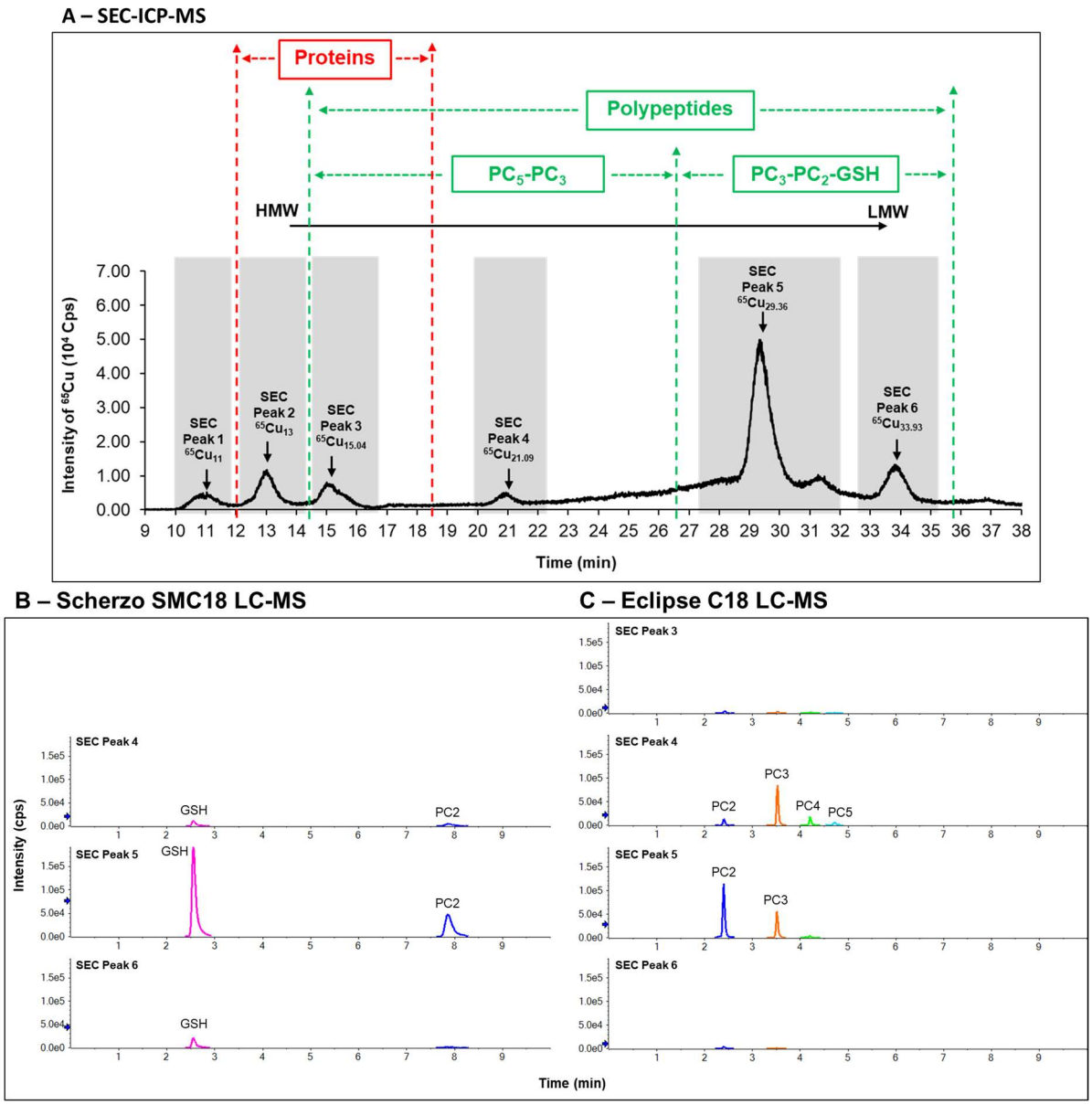

Figure 4: SEC-ICP-MS chromatogram of the separation (A) of ^{65}Cu complexes present in the HSP fraction after 72 h of exposure time of *C. reinhardtii* (acclimated to low-Fe media (L-algae; $[Fe^{3+}]_{free} = 10^{-19}$ M)) to ^{65}Cu ($[^{65}Cu^{2+}]_{free}$ = 39.3 nM) in Fe-replete media. The candidate ligands for the binding of Cu in the HSP fraction were identified by proteomic and peptidomic analyses. Based on these analyses, the colors indicate a rough delineation of the retention times (RT) of the proteins (red) and the (poly)peptides (green) along a molecular weight (MW) gradient (black line) of these biomolecules.